Applied Surface Science 733 (2026) 166599

Contents lists available at ScienceDirect

Applied Surface Science

journal homepage: www.elsevier.com/locate/apsusc

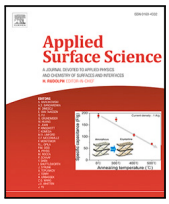

Full length article

Phosphorus-based lubricant additives on iron with Machine Learning Interatomic Potentials

Paolo Restuccia [a],[1], Enrico Pedretti [a],[1], Francesca Benini [a], Sophie Loehlé [b], M. Clelia Righi [a],*

[a] Dipartimento di Fisica e Astronomia, Università di Bologna, Viale Berti Pichat 6/2, Bologna, 40127, Italy
[b] TotalEnergies, OneTech Fuels&Lubricants, Research Center Solaize, Chemin du Canal BP 22, Solaize, 69360, France

ARTICLE INFO

Keywords:
Phosphorus-based additives
Tribofilm formation
Molecular adsorption
Steric effect
Machine learning interatomic potentials

ABSTRACT

Phosphorus-based lubricant additives protect metallic contacts under boundary lubrication by forming surface films that reduce wear and friction. However, the molecular mechanisms driving their friction-reducing effects remain unclear, especially for phosphate esters, whose molecular structure critically impacts tribological behaviour. Here, we employ machine learning–based molecular dynamics simulations to investigate the tribological performance of three representative phosphorus-based additives, Dibutyl Hydrogen Phosphite (DBHP), Octyl Acid Phosphate (OAP), and Methyl Polyethylene Glycol Phosphate (mPEG-P), confined between iron surfaces. DBHP exhibits the lowest friction and largest interfacial separation, combining strong surface reactivity with significant steric hindrance. In contrast, phosphate-based additives show higher friction due to limited steric protection and partial loss of surface coverage under extreme conditions. Systematic variation within the mPEG-P series reveals that increasing ester functionality and chain length reduces friction by enhancing steric separation, even when surface reactivity decreases. These results establish a mechanistic hierarchy in boundary lubrication, where chemical reactivity promotes film formation, while steric architecture primarily controls shear response. These findings provide atomistic guidelines for the rational design of phosphorus-based lubricant additives that balance reactive anchoring with optimized steric structures.

1. Introduction

Lubrication is a fundamental process that enables the reliable operation of mechanical contacts, where friction and wear must be minimized to ensure long-term performance and durability. Among the different lubrication materials, oils containing specific chemical additives are the most widely employed in engineering and industrial applications. These additives are essential components of lubricant formulations, providing functionalities, such as anti-wear, anti-oxidant, and anti-corrosive protection, that base oils alone cannot offer. When the liquid film becomes too thin to sustain the applied load, many sliding components operate under boundary or mixed lubrication regimes. In such conditions, direct asperity contacts can occur, and lubricant additives become the primary agents controlling friction and wear. These molecules adsorb onto the metallic surfaces and undergo mechanochemical reactions that generate protective tribofilms, preventing metal-to-metal contact and reducing interfacial shear [1–3]. Designing advanced additives capable of efficiently performing these functions remains a central challenge in tribology.

Among the wide range of lubricant additives, organic friction modifiers are extensively employed in common engine oils to reduce friction and wear thanks to the formation of incompressible self assembled monolayer [4–6]. Within this class of lubricants, organophosphorus compounds, such as phosphate esters, phosphites, and combined phosphorus/sulphur species, have long been recognized as indispensable ingredients in boundary lubrication. Their remarkable anti-wear and extreme-pressure performance arises from their ability to form protective surface films that simultaneously minimize wear and adjust frictional properties [7,8]. The underlying tribochemical reactions are complex and typically yield a mixture of iron phosphates, polyphosphates, and phosphides, which together protect the interface and lower shear stresses under demanding conditions [9]. As a prerequisite to these processes, tribofilm formation is typically initiated by the adsorption of lubricant additives at the metal surface. In the present work, we focus on elucidating these early-stage adsorption mechanisms for phosphorus-based lubricant additives.

* Corresponding author.
E-mail address: clelia.righi@unibo.it (M.C. Righi).
[1] Authors contributed equally.

https://doi.org/10.1016/j.apsusc.2026.166599
Received 16 December 2025; Received in revised form 23 February 2026; Accepted 12 March 2026
Available online 13 March 2026

Within this chemical family, phosphate esters represent a particularly versatile class whose molecular architecture critically determines their tribological performance. Factors such as alkyl or aryl substitution, chain length, branching, and degree of esterification all influence how these compounds adsorb, react, and decompose under sliding conditions [10,11]. To unravel how molecular structure influences tribological behaviour, three representative phosphorus-based additives are considered: Octyl Acid Phosphate (OAP), Dibutyl Hydrogen Phosphite (DBHP), and Methyl Polyethylene Glycol Phosphate (mPEG-P) whose structures are shown in Fig. 1. Each embodies a distinct structural motif and provides complementary insights into the molecular origins of lubricant performance.

OAP is a monoester phosphate with a relatively long alkyl chain, striking a balance between surface activity and hydrophobicity. Its asymmetric structure, comprising a single octyl group bound to the phosphate group and two acidic hydrogens, enhances both hydrogen bonding and surface reactivity, shaping its adsorption behaviour and the nature of the resulting tribofilm [7]. DBHP, in contrast, is a phosphite additive characterized by a trivalent phosphorus centre with a P = O double bond. This structural feature leads to distinct tribochemical pathways, as phosphites can transform into phosphorus-rich species such as iron phosphides, which are particularly efficient in lowering interfacial shear [9]. mPEG-P, instead, integrates a phosphate ester headgroup with a polyethylene glycol (PEG) tail terminated by a methyl group, producing an amphiphilic molecule that combines hydrophilic PEG chains with hydrophobic termination [12]. Its synthesis typically involves phosphorylation of methyl-terminated PEG followed by hydrolysis or neutralization, yielding mixtures of mono-, di-, and triesters with varying amphiphilicity. The degree of esterification governs the surface affinity: monoesters ($RO–PO_3H_2$) exhibit strong acidity and adsorption on metal oxides, diesters ($(RO)_2–PO_2H$) maintain surface activity with greater hydrophobicity, and triesters ($(RO)_3–PO$) are more soluble in non-polar lubricants but less surface-reactive.

Despite extensive experimental research, a complete understanding of how molecular architecture controls the balance between reactivity, steric effects, and film-forming ability remains elusive. Computational methods, particularly molecular dynamics (MD), have become invaluable in exploring such molecular-scale mechanisms. Recent MD studies have shown that even subtle structural modifications can alter decomposition kinetics and tribofilm composition. For example, branched alkyl substituents accelerate mechanochemical breakdown relative to linear analogues, with tri(s-butyl) phosphate decomposing faster than tri(n-butyl) phosphate owing to larger pre-exponential factors in stress-temperature relationships [13]. Moreover, the substrate composition, like iron versus iron oxide, strongly affects reaction pathways and final tribofilm chemistry [10].

However, conventional classical MD is limited by its inability to capture bond-breaking and electronic effects with quantum accuracy. The recent emergence of machine-learning interatomic potentials (MLPs) bridges this gap, combining near-first-principles accuracy with the efficiency of classical MD. These approaches now allow systematic investigation of how chain length, esterification degree, and steric hindrance govern interfacial reactivity and frictional response under realistic tribological conditions [14,15].

In this work, we leverage these advances to perform a comparative study of DBHP, OAP, and mPEG-P using machine-learning-based molecular dynamics simulations. By correlating molecular structure with frictional behaviour, interfacial separation, and surface chemistry, we aim to uncover the fundamental design principles governing the performance of phosphorus-based lubricant additives. The insights gained from this study are expected to inform the rational development of next-generation lubricant formulations with improved performance and durability.

2. Methods

2.1. Training machine learning interatomic potentials

To perform large scale molecular dynamics simulations of tribological systems while preserving high accuracy in the description of chemical bonding, it is necessary to develop machine learning interatomic potentials (MLIPs) trained on DFT data. This task is inherently challenging, as it requires sampling a broad range of atomic configurations to capture the extreme conditions typically encountered by lubricant mixtures and tribological interfaces in sliding nano-contacts. The accuracy of a MLIP critically depends on the diversity and representativeness of the underlying DFT dataset, making it paramount to include the most relevant conditions across a wide portion of the configurational space.

To address this issue, we adopted an active learning strategy using the Smart Configuration Sampling (SCS) framework developed by our group [16]. SCS enables efficient exploration of the configuration space by performing explorative molecular dynamics in tribological conditions using the evolving MLIP. This allows access to time scales significantly longer than those reachable by ab initio molecular dynamics, enabling to sampling of rare events and highly strained reactive configurations. Through an iterative process, SCS expands the *ab initio* dataset by identifying configurations associated with high model uncertainty during the dynamics and computing their corresponding DFT energies and forces.

The active learning procedure led to the identification of 12 136 *ab initio* configurations, which constitute the final dataset used to train the MLIP. The dataset was randomly divided into 95% training and 5% validation sets. It includes bulk iron structures, Fe(110) and Fe(210) surfaces, isolated molecules, adsorbed species, dissociated fragments, confined molecular layers between iron slabs, and sliding interfacial configurations sampled at different temperatures, normal loads (up to 10 GPa), and sliding velocities representative of the production simulations. This broad sampling ensures coverage of both equilibrium structures and highly strained reactive states relevant to tribological conditions. Iterative retraining within the SCS framework was continued until the validation error on forces reached convergence and remained stable in subsequent cycles. This strategy enhances the transferability of the MLIP to the shear and load regimes encountered in boundary lubrication simulations.

For the MLIP model we employed the DeePMD-kit [17] architecture, using the two-body embedding DeepPot-SE (`se_e2_a`) descriptor with [25, 50, 100] neurons, and a fitting net containing [120, 120, 120] neurons. Fig. 2 shows the model's accuracy in predicting atomic forces on the whole dataset (whose systems are detailed in Section 2.3), achieving a root mean square error (RMSE) of 0.18 eV/Å. A detailed breakdown of the model accuracy for each subsystem included in the dataset is provided in Section 1 of the Supplementary Materials (SM). We further validated the MLIP against relevant physical quantities, including adsorption and dissociative adsorption energies of the different molecules on Fe(110) surfaces, obtaining excellent agreement with DFT results (see Section 2 of the SM). This level of accuracy is consistent with state-of-the-art MLIPs: recent benchmarks demonstrate that RMSEs of this magnitude enable accurate simulations of complex systems while maintaining computational efficiency [18]. Moreover, error analyses confirm that force RMSEs in the range of 0.15–0.4 eV/Å are widely considered acceptable for reliable predictive modelling [19].

2.2. Set up ab initio calculations

All the *ab initio* calculations were performed using spin-polarized DFT as implemented in the GPU-enabled version of the Quantum Espresso computational suite [20]. We adopted the same computational parameters for all the considered systems, following standard practice in MLIP development. To ensure these shared settings yielded

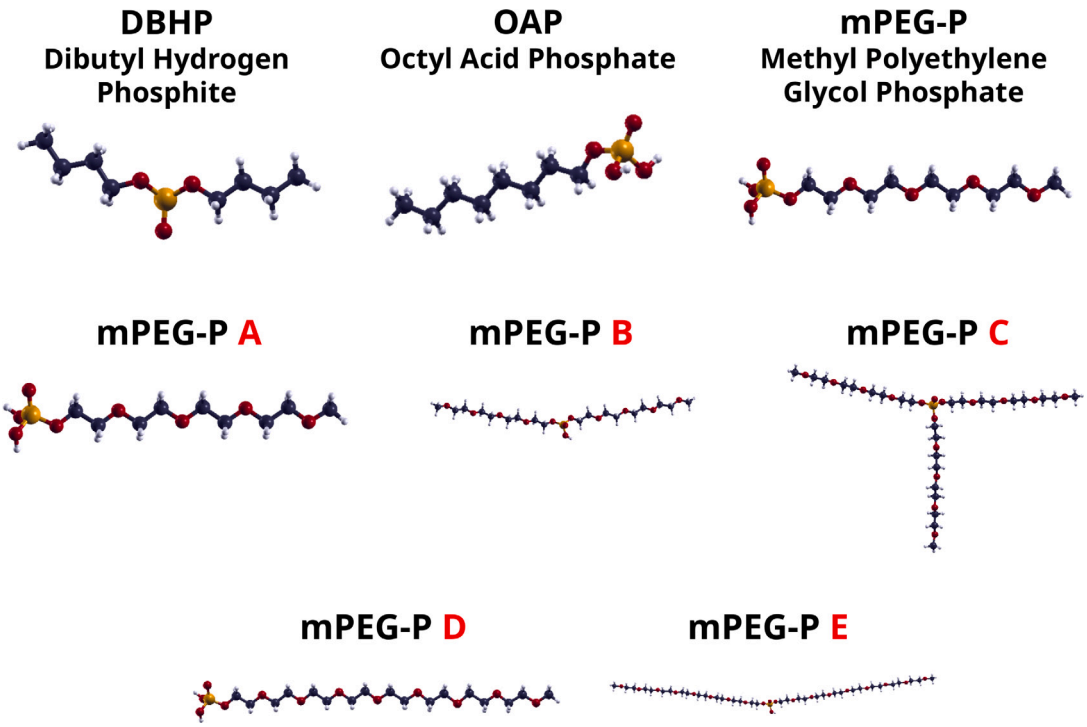

Fig. 1. Ball-and-stick representation of the molecules studied in this work. From now on, white atoms represent H, grey C, yellow P and red O, respectively. In the lower panels, mPEG-P molecules with different number of esters and glycol units are shown. We modelled mPEG-P monoester with 4 glycol units (label A in red), mPEG-P diester with 4 glycol units (label B), mPEG-P triester with 4 glycol units (label C), mPEG-P monoester with 8 glycol units (label D), and mPEG-P diester with 8 glycol units (label E).

reliable results across the different active learning simulations, we used sufficiently large simulation cells to minimize discrepancies between systems. In particular, the general gradient approximation (GGA) within the Perdew–Burke–Ernzerhof (PBE) parametrization was used to describe the exchange and correlation functional. The projector–augmented wave (PAW) was used to model the interaction between valence electrons and ions plus core electrons, whereas we employed the ultrasoft method for the Fe atoms to lower the cut-off threshold for the wave functions' basis set. The energy (density) cutoff of the plane–wave expansion was set to 60 Ry (480 Ry), with a Gaussian smearing of 0.00735 Ry and a convergence threshold for the electronic self-consistent loop equal to 10^{-6} Ry, while we sampled the Brillouin zone with a **k**-spacing of 0.1 $Å^{-1}$. To take into account van der Waals dispersive forces, we used the DFT-D3 approach developed by Grimme et al. [21].

2.3. Molecular systems and large-scale simulations set up

We investigated three molecules for our molecular dynamics simulations, namely dibutyl hydrogen phosphite (DBHP), octyl acid phosphate (OAP) and methyl polyethylene glycol phosphate (mPEG-P) ester, as illustrated in Fig. 1. As discussed in the Introduction, lubricant formulations typically contain a mixture of mono-, di-, and triester forms of mPEG-Ps, which were also included in our study (shown in Fig. 1). The additives were confined between an asymmetric iron interface, composed of Fe(110) and Fe(211) surfaces, featuring a single asperity and an in-plane area of 20.93 nm × 4.87 nm, which is represented in Fig. 3. This setup, previously employed in tribological simulations [22], assures the modelling of a more realistic, non-flat contact interface.

To model extreme boundary lubrication conditions, we isolated the effect of lubricant additives by excluding the base oil from our simulations. In this regime, the external load is large enough to expel most of the liquid lubricant from the contact, leaving only absorbed molecular additives at the interface. This approach allows to focus on the intrinsic tribochemical reactivity and steric effects of the additives under severe confinement.

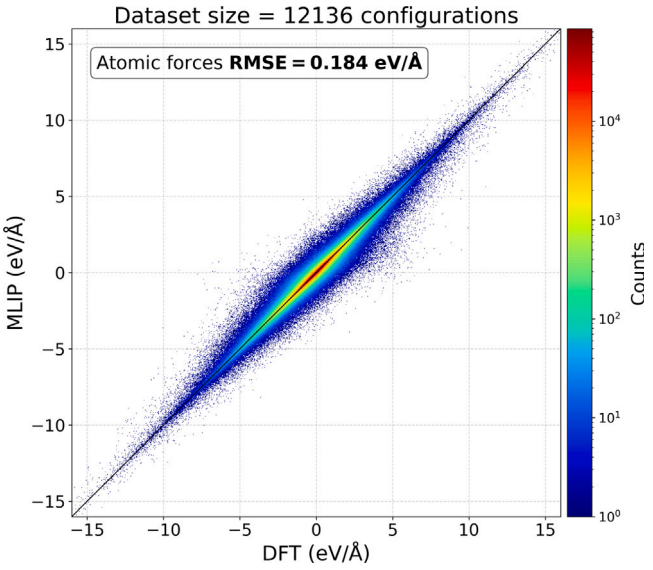

Fig. 2. Parity plot for the DeePMD model evaluated on the complete dataset, comparing predicted atomic forces from the MLIP (y-axis) with reference DFT values. (x-axis). The colour scale indicates the density of data points, with warmer (cooler) colours representing higher (lower) counts of occurrences at specific force values. The overall RMSE is also reported in the plot.

We note that the absence of base oil represents a simplification of real lubricant formulations. Although solvent molecules can influence adsorption equilibria and reaction kinetics, ultimately the load-bearing and friction-reducing behaviour under extreme boundary lubrication

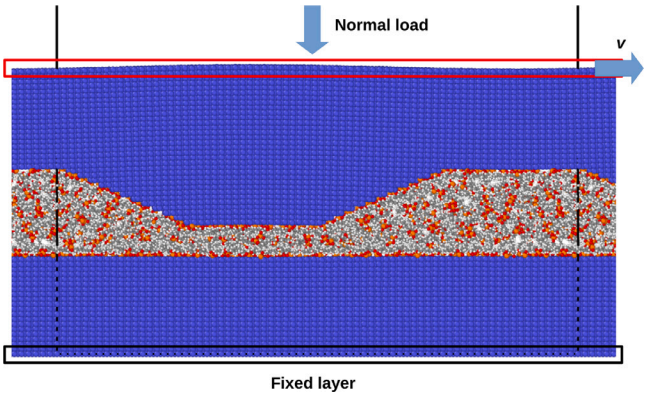

Fig. 3. Ball-and-stick representation of the computational setup for the system containing DBHP molecules confined within the iron interface (represented in blue). The black solid line represents the adopted simulation cell size. The red solid box represents the top-most iron layer where the normal load and the sliding velocity are applied, while the bottom-most black solid box identifies the reference iron layer, with fixed atomic positions.

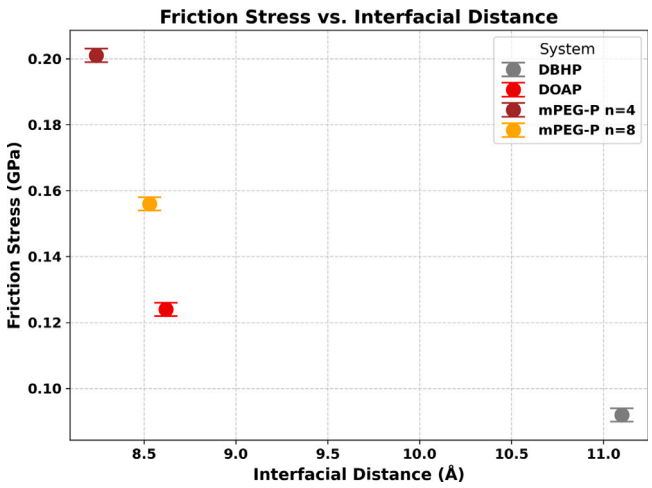

Fig. 4. Friction vs. distance for the systems containing mPEG-P monoester (n = 4), mPEG-P monoester (n = 8), OAP and DBHP. Error bars represent the standard error of the mean (SE), estimated accounting for temporal correlations (see Methods).

conditions is primarily governed by the adsorbed additive-derived interfacial film. Therefore, the present simulations are intended to capture mechanistic trends and relative performance among additives, rather than reproduce absolute friction values under fully formulated lubricant conditions.

For each additive, preliminary calculations were performed to determine the amount of additives necessary to prevent the interfacial cold welding and eliminate voids within the interface. The optimal total molecular mass was approximately 132,800 atomic mass units, corresponding to 688 molecules of DBHP, 632 of OAP and 461 of the monoester mPEG-P. This setup resulted in simulation cells containing approximately 100,000 atoms across all systems.

All the large-scale molecular dynamics simulations were carried out using the LAMMPS package [23] interfaced with DeePMD. We adopted a consistent simulation protocol across all system: the lubricant additives were initially placed randomly within the iron interface, followed by a system relaxation. The system was then linearly heated to the target temperature of 300 K using a timestep of 1 fs. After thermalization, we configured the set up to model the non-equilibrium tribological interface under combined load and shear conditions. Specifically, we applied an NVT ensemble to the bulk iron layers and an NVE ensemble to the interfacial region. The bottommost layer of the lower iron surface was kept fixed, while a constant normal load of 1 GPa and a sliding velocity of 5 m/s were imposed on the topmost layer of the upper surface. Although higher than typical nominal macroscopic pressures, the applied value is representative of local asperity-level contact stresses that can transiently arise under extreme boundary lubrication conditions.

The imposed sliding velocity lies at the upper range of experimental values. However, such conditions are routinely adopted in molecular dynamics simulations to enable the observation of tribochemical reactions within the nanosecond time scales accessible to machine-learning-based MD. Because the intrinsic atomic velocities associated with bond breaking and structural rearrangements are orders of magnitude higher than the externally imposed sliding speed, the latter mainly influences the frequency at which reactive events are sampled, without modifying the fundamental dissociation pathways.

The reported friction stress corresponds to the time average over the final 1 ns of the sliding trajectory. The associated uncertainty is given as the standard error (SE) of the average, computed accounting for temporal correlations in the force time series [24]. The integrated autocorrelation time, estimated from the normalized autocorrelation function, is approximately 0.1 ps, yielding an effective sample size of around 5000 statistically independent configurations. The resulting SE is approximately 0.0025 GPa.

2.4. Number of bonds per molecule (NBM) definition

Due to the high number of dissociation events observed in our MD simulations, which is significantly larger than in our previous works [25–27], we introduced a descriptor called the number of bonds per molecule (NBM). This metric quantifies the average number of bonds for a specific type formed over time by a single molecule. For example, in the case of OAP, each molecule contains one phosphorus atom that forms four P–O bonds. The corresponding NBM for the P–O bond type is therefore 4, indicating that each molecule, on average, forms four of these bonds, as shown in Fig. 1. In more complex cases, like the O–H bond in the OAP or mPEG-P where multiple oxygen and atoms are present, the NBM is equal to 2, reflecting the two O–H bonds typically found in each molecule.

The NBM is computed by multiplying the coordination number (CN) of a given bond type by the number of atoms for a specific atomic type. The CN is calculated by integrating the pair radial distribution function $g(r)$ up to the first minimum beyond the main peak, corresponding to the first coordination shell. It is defined mathematically as:

$$CN = 4\pi \int_0^{r_{min}} \rho \cdot g(r) \cdot r^2 dr \tag{1}$$

where ρ is the atomic number density of the system, and r_{min} is the position of the first minimum in the $g(r)$. This integration yields the average number of neighbouring atoms surrounding a reference atom within the first coordination shell. This approach allows to monitor the dissociation events of each bond type and to compare the distinct dissociative behaviours of the molecular additives under study. This descriptor provides a statistically averaged measure of coordination changes and is primarily intended to capture global trends in bond formation and dissociation across different systems. By construction, it does not resolve highly localized or rare reaction events occurring at specific atomic sites. Therefore, detailed mechanistic insights are obtained through direct inspection of the atomistic trajectories, while the NBM serves as a comparative metric to assess relative reactivity.

3. Results and discussion

3.1. Difference between phosphites and phosphates as friction modifiers

To elucidate the origin of the distinct tribological behaviour of phosphites and phosphates, we first analyze the relationship between

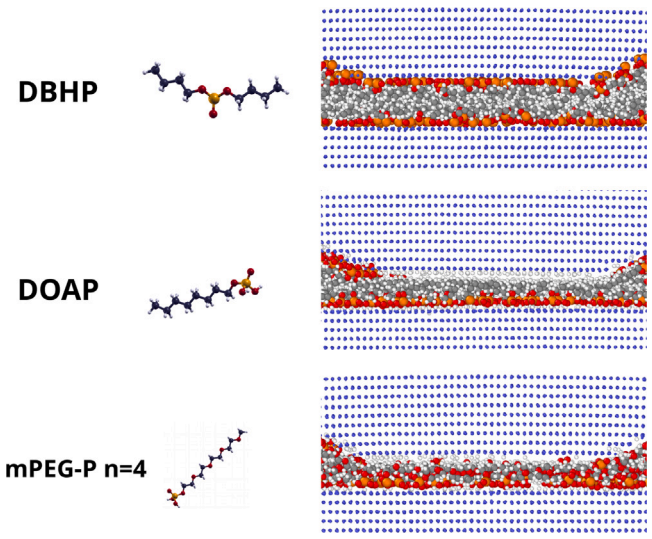

Fig. 5. Ball-and-stick representation of the iron asperity containing DBHP (upper panel), OAP (central) and mPEG-P monoester with 4 glycol units (lower) additives at the end of the sliding simulations (19.5 ns). The dimension of Fe atoms has been reduced to make more visible the interaction of the P-based additives.

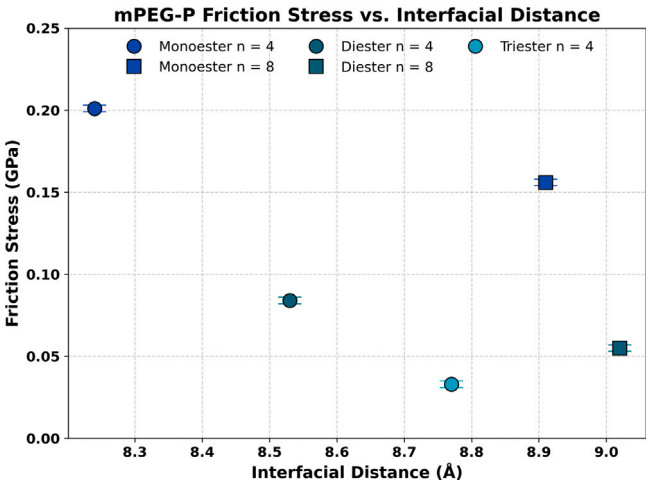

Fig. 6. Friction vs. distance for the systems containing mPEG-P monoester with 4 (8) glycol units (label A (D) in Fig. 1), diester with 4 (8) glycol units (label B (E) in Fig. 1) and triester with 4 glycol units (label C in Fig. 1). Error bars represent the standard error of the mean (SE), estimated accounting for temporal correlations (see Methods).

friction stress and interfacial separation during sliding. This comparison establishes a direct link between the macroscopic frictional response and nanoscale structure of the interfacial film, and has been successfully used to investigate the tribological behaviour of different additives [15]. As shown in Fig. 4, the interface lubricated by DBHP exhibits the largest interfacial separation and lowest friction among the tested additives. This inverse trend between boundary film thickness and friction is consistent with prior observations that thicker tribofilms reduce shear [28]. Notably, DBHP maintains a significantly larger separation (around 11 Å), whereas OAP and mPEG-P cluster around 8.5 Å. These results further confirm that phosphites and phosphates lead to markedly different frictional responses under identical sliding conditions [9].

To understand the structural origin of these differences, we examine the interfacial configurations at the end of sliding (Fig. 5). DBHP molecules adsorb uniformly across both the asperity tip and the counter surface, whereas OAP and mPEG-P predominantly adhere to the lower substrate. Additionally, the bulkier DBHP alkyl chains introduce greater steric hindrance compared to OAP and mPEG-P additives, further increasing the interfacial separation and reducing direct asperity–asperity interactions. This structural effect suggests that steric architecture plays a significant role in controlling the mechanical response under sliding. This qualitative behaviour is supported by quantitative data: DBHP exhibits higher molecular and dissociative adsorption energies, as reported in a recent study on phosphorus-based additives [29]. More generally, strong chemisorption of organophosphorus additives on iron substrates is well documented in the literature, with surface reactions yielding polyphosphate-rich films (phosphates) [13] or P-rich species (phosphites) [30].

In addition to molecule–surface bonding, friction-induced reactions between additive molecules may contribute to the evolution and cohesion of the tribofilm. In the present simulations, limited formation of short phosphorus-containing species, including incipient polyphosphate-like fragments in the case of DBHP, was observed. However, these species remain localized and do not develop into an extended network within the simulated time scale. As a result, the dominant mechanisms governing shear response in our simulations are surface anchoring and steric hindrance rather than extensive intermolecular crosslinking. We note that the formation of more extended polyphosphate networks may occur under different environmental conditions or longer time scales than those accessible in the present simulations. The interplay between intermolecular polymerization and shear strength therefore represents an important topic for further investigation.

To further clarify whether the observed differences arise solely from structural effects or also involve distinct chemical reactivity, we analyze the evolution of the normalized bond metrics (NBM) during sliding. Among the three additives, DBHP is the only one to exhibit significant P–O bond dissociation (−16% from the beginning to the end of the simulation). In contrast, both OAP and mPEG-P esters show substantial O–H bond dissociation (−50% for OAP and −35% for mPEG-P), associated with deprotonation of the phosphate acid head group. All additives display an increase in O–Fe bond formation, albeit via different mechanisms. For DBHP, the increase (+71%) results from P–O dissociation, which exposes reactive oxygen atoms capable of bonding to iron. For OAP (+78%) and mPEG-P (+50%), O–Fe bonds increase primarily due to hydrogen release, leaving oxygen atoms available for surface coordination. These results confirm that DBHP exhibits distinct tribochemical reactivity compared to phosphate-based additives.

Taken together, the structural and chemical analyses indicate that steric effects and tribochemical reactivity operate at complementary but distinct levels. The enhanced reactivity of DBHP promotes strong chemisorption and the formation of a stable interfacial layer, ensuring robust surface anchoring. However, the pronounced friction reduction correlates more directly with the increased interfacial separation induced by its bulky alkyl chains, which mitigate direct contact between opposing asperities and lower shear stress. Thus, while chemical reactivity governs film formation and anchoring, steric architecture appears to play the dominant role in determining frictional performance under extreme boundary lubrication conditions.

3.2. Different number of ester groups and chain length in mPEG-P

To disentangle the respective roles of steric architecture and chemical reactivity in friction reduction, we systematically analyze the mPEG-P series by varying the number of ester groups and the chain length. The resistive force (friction stress) and corresponding interfacial separation for each variant of mPEG-P in the last 1 ns of sliding are reported in Fig. 6. Two systematic trends emerge: for fixed chain length, increasing the number of ester groups (going from monoester

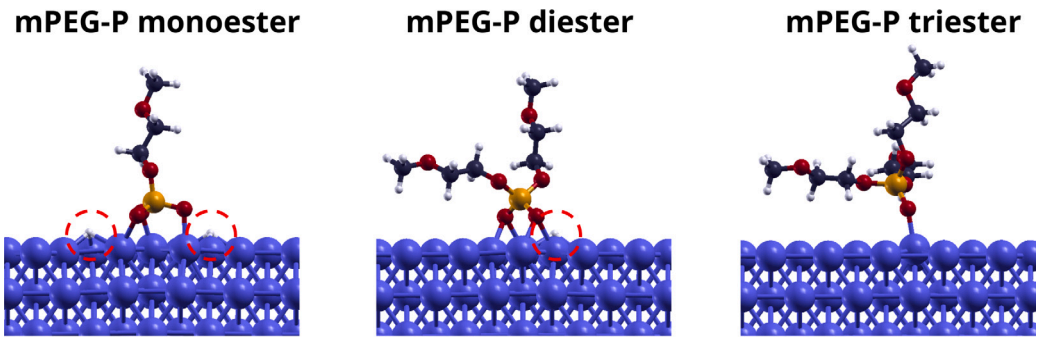

ADDITIVE	E_{DISS} (eV)	E_{DISS} (eV) with vdW
Monoester	–2.73	–3.28
Diester	–2.00	–2.64
Triester	–0.69	–1.36

Fig. 7. H- dissociative adsorption energy mPEG-P (n = 1) mono-, di- and triester over a Fe(110) substrate.

to triester) leads to lower friction and larger interfacial separation. Similarly, for fixed number of ester groups, increasing the chain length results in increased separation and reduced friction. These results indicate that the molecular architecture has a direct impact on the mechanical response of the confined interface.

The observed trends point to a dominant steric contribution: larger numbers of hydrocarbon chains and longer backbones enhance steric hindrance, improving slipperiness and load carrying capacity. Notably, increasing the number of ester groups produces a pronounced friction decrease even when the corresponding increase in separation is moderate, whereas increasing chain length mainly enlarges the interfacial distance with a comparatively smaller friction reduction. This behaviour is consistent with polymer-brush steric lubrication mechanisms, in which densely tethered chains resist compression, maintain separation, and shear at low stress, thereby lowering the friction coefficient under boundary/mixed lubrication regimes [31–33]. Moreover, increasing ester functionality in base-oil esters has been shown to thicken adsorbed films and reduce friction [34], confirming that multi-ester architectures promote separation and lower shear.

Collectively, these findings establish a clear mechanistic hierarchy in phosphorus-based boundary lubrication: chemical reactivity enables surface anchoring, whereas steric architecture ultimately controls interfacial separation and frictional response. These mechanistic insights suggest clear pathways for experimental validation. Post-mortem surface analyses of tribological tests, for example by X-ray photoelectron spectroscopy (XPS), could be used to characterize the chemical composition of the resulting tribofilms, allowing direct assessment of phosphite- versus phosphate-derived surface phases. In parallel, controlled tribological experiments using additives with different ester functionality and chain length would enable direct comparison with the predicted steric trends, providing a one-to-one validation of the relationship between molecular architecture, interfacial separation, and frictional performance. Such combined experimental–computational approaches could facilitate the rational design of next-generation phosphorus-based lubricant formulations.

Interestingly, the systematic friction reduction contrasts with the adsorption behaviour of the mPEG-P molecules on the iron substrate. The evolution of the O–Fe NBM, used as a proxy for surface attachment, shows a sharper increase for monoesters (+50%) than for the diesters (+16%) and triesters (+8%). This result indicates that monoesters adhere more readily to the surface, despite exhibiting higher friction.

DFT calculations of O–H dissociative adsorption energies (Fig. 7) are consistent with this trend: mPEG-P mono- and diesters display significantly stronger adsorption via hydroxyl dissociation (by a factor 4 and 3, respectively) compared to the triester, which lacks O–H groups. This behaviour aligns with established understanding that monoesters with acidic O–H groups typically enhance chemisorption on Fe/Fe-oxide more effectively than diesters/triesters [35].

Taken together, these results reveal that stronger surface reactivity does not necessarily translate into lower friction. Within the mPEG-P series, increasing steric bulk reduces friction even when the tendency for dissociative adsorption and chemisorption decreases. This confirms that chemical reactivity primarily governs film formation and surface anchoring, whereas steric architecture plays the dominant role in controlling interfacial separation and shear response under boundary lubrication conditions.

The triester variant of mPEG-P with chain length n = 8 was not included in the comparison due to its large molecular size. First, its lateral dimensions approach the size of the simulation cell, potentially introducing periodic confinement artifacts. Second, maintaining a comparable total molecular mass would require too few molecules to ensure statistically meaningful results.

4. Conclusions

This work employed machine learning-based molecular dynamics to investigate the tribological behaviour of phosphorus-based lubricant additives (DBHP, OAP, and mPEG-P esters), under boundary lubrication conditions, with particular attention to the role of molecular architecture.

DBHP exhibits the lowest friction and largest interfacial separation compared to OAP and mPEG-P monoesters, resulting from the combined effect of enhanced steric hindrance and strong tribochemical reactivity. However, the comparative analysis indicates that while chemical reactivity promotes surface anchoring and film formation, steric architecture plays a dominant role in governing interfacial separation and shear response.

Within the mPEG-P series, friction decreases systematically with increasing esterification degree and chain length, despite a reduced tendency for dissociative adsorption. This trend further supports a steric-dominant lubrication mechanism under extreme confinement.

Overall, our findings highlight that under extreme confinement, steric hindrance and molecular architecture can outweigh surface reactivity in determining lubricant performance. The combination of machine learning-based MD and bond-metric analysis provides atomistic insight into the balance between adsorption, decomposition, and steric effects. These results outline design guidelines for next-generation phosphorus-based additives, highlighting the importance of balancing reactive anchoring groups with sufficient steric bulk to achieve durable and low-friction interfaces.

CRediT authorship contribution statement

Paolo Restuccia: Writing – original draft, Investigation, Formal analysis. **Enrico Pedretti:** Writing – review & editing, Investigation, Formal analysis. **Francesca Benini:** Methodology, Investigation. **Sophie Loehlé:** Writing – review & editing, Supervision, Conceptualization. **M. Clelia Righi:** Writing – review & editing, Supervision, Funding acquisition, Conceptualization.

Declaration of competing interest

The authors declare that they have no known competing financial interests or personal relationships that could have appeared to influence the work reported in this paper.

Acknowledgements

MCR, PR, EP, and FB acknowledge the SLIDE project, which received funding from the European Research Council (ERC) under the European Union's Horizon 2020 research and innovation program. (Grant Agreement No. 865633). We also acknowledge the CINECA award under the ISCRA initiative, for the availability of high-performance computing resources and support.

Appendix A. Supplementary data

Supplementary material related to this article can be found online at https://doi.org/10.1016/j.apsusc.2026.166599.

Data availability

Data will be made available on request.

References

[1] H. Spikes, Low- and zero-sulphated ash, phosphorus and sulphur anti-wear additives for engine oils, Lubr. Sci. 20 (2) (2008) 103–136, http://dx.doi.org/10.1002/ls.57, URL https://onlinelibrary.wiley.com/doi/abs/10.1002/ls.57.

[2] Z. Tang, S. Li, A review of recent developments of friction modifiers for liquid lubricants (2007–present), Curr. Opin. Solid State Mater. Sci. 18 (3) (2014) 119–139, http://dx.doi.org/10.1016/j.cossms.2014.02.002, URL https://www.sciencedirect.com/science/article/pii/S1359028614000059.

[3] O. Furlong, F. Gao, P. Kotvis, W. Tysoe, Understanding the tribological chemistry of chlorine-, sulfur- and phosphorus-containing additives, Tribol. Int. 40 (5) (2007) 699–708, http://dx.doi.org/10.1016/j.triboint.2006.05.011, URL https://www.sciencedirect.com/science/article/pii/S0301679X06002040.

[4] X. Yi, H. Xu, G. Jin, Y. Lu, B. Chen, S. Xu, J. Shi, X. Fan, Boundary slip and lubrication mechanisms of organic friction modifiers with effect of surface moisture, Friction 12 (7) (2024) 1483–1498, http://dx.doi.org/10.1007/s40544-023-0820-0, URL https://link.springer.com/article/10.1007/s40544-023-0820-0.

[5] S. Xu, Y. Yu, Z. Wang, H. Li, S. Li, J. Lu, J. Shi, Effect of the combination of antioxidant and dispersant in traction oils on their interaction and lubricating property, Tribol. Int. 198 (2024) 109844, http://dx.doi.org/10.1016/j.triboint.2024.109844, URL https://www.sciencedirect.com/science/article/pii/S0301679X24005966.

[6] J. Shi, H. Li, Y. Lu, L. Sun, S. Xu, X. Fan, Synergistic lubrication of organic friction modifiers in boundary lubrication regime by molecular dynamics simulations, Appl. Surf. Sci. 623 (2023) 157087, http://dx.doi.org/10.1016/j.apsusc.2023.157087, URL https://www.sciencedirect.com/science/article/pii/S016943322300764X.

[7] D.W. Johnson, The tribology and chemistry of phosphorus-containing lubricant additives, in: P.H. Darji (Ed.), Advances in Tribology, IntechOpen, London, 2016, http://dx.doi.org/10.5772/63654, URL https://www.intechopen.com/chapters/51177.

[8] A. Emmanuel, P. Onu, A.A. Adesoji, A. Adediran, O.J. Ogunniyi, S.L. Lawal, S.I. Monye, The role of additives in enhancing the tribological properties of lubricants, in: 2024 International Conference on Science, Engineering and Business for Driving Sustainable Development Goals, SEB4SDG, 2024, pp. 1–11, http://dx.doi.org/10.1109/SEB4SDG60871.2024.10630241, URL https://ieeexplore.ieee.org/document/10630241.

[9] M.I. De Barros-Bouchet, M.C. Righi, D. Philippon, S. Mambingo-Doumbe, T. Le-Mogne, J.M. Martin, A. Bouffet, Tribochemistry of phosphorus additives: experiments and first-principles calculations, RSC Adv. 5 (2015) 49270–49279, http://dx.doi.org/10.1039/C5RA00721F, URL https://pubs.rsc.org/en/content/articlelanding/2015/ra/c5ra00721f.

[10] Q. Yang, F. Duan, Tribological properties of phosphate ester confined between iron-based surfaces, Langmuir 40 (7) (2024) 3738–3747, http://dx.doi.org/10.1021/acs.langmuir.3c03464.

[11] X. Wu, G. Zhao, X. Wang, W. Liu, W. Liu, Treelike polymeric phosphate esters grafted onto graphene oxide and its tribological properties in polyalkylene glycol for steel/steel contact at elevated temperature, RSC Adv. 6 (2016) 47824–47832, http://dx.doi.org/10.1039/C6RA06919C.

[12] S. Penczek, K. Kaluzynski, B. Wisniewski, J. Pretula, R. Szymanski, G. Lapienis, The MPEG monophosphate ester: Synthesis and characterization, J. Biomater. Sci. Polym. Ed. 20 (14) (2009) 2103–2116, http://dx.doi.org/10.1163/156856208X400483.

[13] C. Ayestarán Latorre, J.E. Remias, J.D. Moore, H.A. Spikes, D. Dini, J.P. Ewen, Mechanochemistry of phosphate esters confined between sliding iron surfaces, Commun. Chem. 4 (1) (2021) 178, http://dx.doi.org/10.1038/s42004-021-00615-x, URL https://www.nature.com/articles/s42004-021-00615-x.

[14] A. Pacini, M. Ferrario, S. Loehle, M.C. Righi, Advancing tribological simulations of carbon-based lubricants with active learning and machine learning molecular dynamics, Eur. Phys. J. Plus 139 (6) (2024) 549, http://dx.doi.org/10.1140/epjp/s13360-024-05348-z, URL https://link.springer.com/article/10.1140/epjp/s13360-024-05348-z.

[15] H.T.T. Ta, M. Ferrario, S. Loehlé, M.C. Righi, Probing additives for green lubricants with the aid of machine learning molecular dynamics: The case of gallate molecules for aqueous solutions, Appl. Surf. Sci. 695 (2025) 162836, http://dx.doi.org/10.1016/j.apsusc.2025.162836, URL https://www.sciencedirect.com/science/article/pii/S0169433225005501.

[16] A. Pacini, M. Ferrario, M.C. Righi, Accelerating data set population for training machine learning potentials with automated system generation and strategic sampling, J. Chem. Theory Comput. 21 (14) (2025) 7102–7110, http://dx.doi.org/10.1021/acs.jctc.5c00616, URL https://pubs.acs.org/doi/full/10.1021/acs.jctc.5c00616.

[17] J. Zeng, D. Zhang, D. Lu, P. Mo, Z. Li, Y. Chen, M. Rynik, L. Huang, Z. Li, S. Shi, Y. Wang, H. Ye, P. Tuo, J. Yang, Y. Ding, Y. Li, D. Tisi, Q. Zeng, H. Bao, Y. Xia, J. Huang, K. Muraoka, Y. Wang, J. Chang, F. Yuan, S.L. Bore, C. Cai, Y. Lin, B. Wang, J. Xu, J.-X. Zhu, C. Luo, Y. Zhang, R.E.A. Goodall, W. Liang, A.K. Singh, S. Yao, J. Zhang, R. Wentzcovitch, J. Han, J. Liu, W. Jia, D.M. York, W. E, R. Car, L. Zhang, H. Wang, DeePMD-kit v2: A software package for deep potential models, J. Chem. Phys. 159 (5) (2023) 054801, http://dx.doi.org/10.1063/5.0155600, URL https://pubs.aip.org/aip/jcp/article/159/5/054801/2904916/0.

[18] W. Liang, J. Zeng, D.M. York, L. Zhang, H. Wang, Learning DeePMD-Kit: A guide to building deep potential models, in: A Practical Guide To Recent Advances in Multiscale Modeling and Simulation of Biomolecules, AIP Publishing LLC, 2023, http://dx.doi.org/10.1063/9780735425279_006, URL https://pubs.aip.org/books/monograph/137/chapter-abstract/58881185/Learning-DeePMD-Kit-A-Guide-to-Building-Deep.

[19] Y. Liu, X. He, Y. Mo, Discrepancies and error evaluation metrics for machine learning interatomic potentials, Npj Comput. Mater. 9 (1) (2023) 174, http://dx.doi.org/10.1038/s41524-023-01123-3, URL https://www.nature.com/articles/s41524-023-01123-3.

[20] P. Giannozzi, O. Baseggio, P. Bonfà, D. Brunato, R. Car, I. Carnimeo, C. Cavazzoni, S. de Gironcoli, P. Delugas, F. Ferrari Ruffino, A. Ferretti, N. Marzari, I. Timrov, A. Urru, S. Baroni, Quantum ESPRESSO toward the exascale, J. Chem. Phys. 152 (15) (2020) 154105, http://dx.doi.org/10.1063/5.0005082, URL https://pubs.aip.org/aip/jcp/article/152/15/154105/1058748/2.

[21] S. Grimme, J. Antony, S. Ehrlich, H. Krieg, A consistent and accurate ab initio parametrization of density functional dispersion correction (DFT-D) for the 94 elements H-Pu, J. Chem. Phys. 132 (15) (2010) 154104, http://dx.doi.org/10.1063/1.3382344, URL https://pubs.aip.org/aip/jcp/article/132/15/154104/926936/4.

[22] A. Codrignani, S. Peeters, H. Holey, F. Stief, D. Savio, L. Pastewka, G. Moras, K. Falk, M. Moseler, Toward a continuum description of lubrication in highly pressurized nanometer-wide constrictions: The importance of accurate slip laws, Sci. Adv. 9 (48) (2023) eadi2649, http://dx.doi.org/10.1126/sciadv.adi2649, URL https://www.science.org/doi/abs/10.1126/sciadv.adi2649.

[23] A.P. Thompson, H.M. Aktulga, R. Berger, D.S. Bolintineanu, W.M. Brown, P.S. Crozier, P.J. in 't Veld, A. Kohlmeyer, S.G. Moore, T.D. Nguyen, R. Shan, M.J. Stevens, J. Tranchida, C. Trott, S.J. Plimpton, LAMMPS - a flexible simulation tool for particle-based materials modeling at the atomic, meso, and continuum scales, Comput. Phys. Comm. 271 (2022) 108171, http://dx.doi.org/10.1016/j.cpc.2021.108171, URL https://www.sciencedirect.com/science/article/pii/S0010465521002836.

[24] H. Flyvbjerg, H.G. Petersen, Error estimates on averages of correlated data, J. Chem. Phys. 91 (1) (1989) 461–466, http://dx.doi.org/10.1063/1.457480, URL https://pubs.aip.org/aip/jcp/article/91/1/461/91554/.

[25] G. Zilibotti, S. Corni, M.C. Righi, Load-induced confinement activates diamond lubrication by water, Phys. Rev. Lett. 111 (2013) 146101, http://dx.doi.org/10.1103/PhysRevLett.111.146101, URL https://link.aps.org/doi/10.1103/PhysRevLett.111.146101.

[26] S. Loehlé, M.C. Righi, Ab initio molecular dynamics simulation of tribochemical reactions involving phosphorus additives at sliding iron interfaces, Lubricants 6 (2) (2018) 31, http://dx.doi.org/10.3390/lubricants6020031, URL https://www.mdpi.com/2075-4442/6/2/31.

[27] P. Restuccia, M. Ferrario, M. Righi, Monitoring water and oxygen splitting at graphene edges and folds: Insights into the lubricity of graphitic materials, Carbon 156 (2020) 93–103, http://dx.doi.org/10.1016/j.carbon.2019.09.040, URL https://www.sciencedirect.com/science/article/pii/S0008622319309455.

[28] J. Dawczyk, N. Morgan, J. Russo, H. Spikes, Film thickness and friction of ZDDP tribofilms, Tribol. Lett. 67 (2) (2019) 34, http://dx.doi.org/10.1007/s11249-019-1148-9, URL https://link.springer.com/article/10.1007/s11249-019-1148-9.

[29] F. Benini, P. Restuccia, S. Loehlé, Q. Arnoux, M.C. Righi, Combined *ab initio* and experimental study of phosphorus-based anti-wear additives interacting with iron and iron oxide, 2025.

[30] F. Gao, O. Furlong, P.V. Kotvis, W.T. Tysoe, Reaction of tributyl phosphite with oxidized iron: Surface and tribological chemistry, Langmuir 20 (18) (2004) 7557–7568, http://dx.doi.org/10.1021/la049438t, URL https://pubs.acs.org/doi/full/10.1021/la049438t.

[31] W. Yang, F. Zhou, Polymer brushes for antibiofouling and lubrication, Biosurface Biotribology 3 (3) (2017) 97–114, http://dx.doi.org/10.1016/j.bsbt.2017.10.001, URL https://www.sciencedirect.com/science/article/pii/S2405451817300181.

[32] T.A. Gmür, J. Mandal, J. Cayer-Barrioz, N.D. Spencer, Towards a polymer-brush-based friction modifier for oil, Tribol. Lett. 69 (4) (2021) 124, http://dx.doi.org/10.1007/s11249-021-01496-w, URL https://link.springer.com/article/10.1007/s11249-021-01496-w.

[33] M.A. Abdelbar, J.P. Ewen, D. Dini, S. Angioletti-Uberti, Polymer brushes for friction control: Contributions of molecular simulations, Biointerphases 18 (1) (2023) 010801, http://dx.doi.org/10.1116/6.0002310.

[34] K. Hirata, M. Murashima, N. Umehara, T. Tokoroyama, N. Hashizume, W.-Y. Lee, D. Takekawa, K. Narita, Clarification of the effects of adsorption films of ester-blended oil on friction by in situ reflectance spectroscopy, Tribol. Int. 187 (2023) 108718, http://dx.doi.org/10.1016/j.triboint.2023.108718, URL https://www.sciencedirect.com/science/article/pii/S0301679X23005066.

[35] H. Koshima, A. Hamano, H. Tokairin, Y. Murakami, H. Washizu, Experimental and theoretical study on the tribological characteristics of organophosphates on metal surfaces, Tribol. Online 19 (1) (2024) 11–22, http://dx.doi.org/10.2474/trol.19.11, URL https://www.jstage.jst.go.jp/article/trol/19/1/19_11/_article.